Electronic and structural properties, and hyperfine interactions at Sc sites in the semiconductor Sc_2O_3: TDPAC and *ab initio* study

D. Richard,[1] E. L. Muñoz,[1] T. Butz,[2] L. A. Errico,[1,3] and M. Rentería[1]

[1]*Departamento de Física-IFLP (CONICET-UNLP), Facultad de Ciencias Exactas, UNLP, CC 67, 1900 La Plata, Argentina*

[2]*Fakultät für Physik und Geowissenschaften, Institut für Experimentelle Physik II, Universität Leipzig, Linnéstrasse 5, 04103 Leipzig, Germany*

[3]*Universidad Nacional del Noroeste Bonaerense (UNNOBA), Monteagudo 2772, (2700) Pergamino, Argentina*

(Received 4 May 2010; revised manuscript received 18 June 2010; published 15 July 2010)

The time-differential γ-γ perturbed-angular-correlation (TDPAC) technique using $^{44}Ti \rightarrow {}^{44}Sc$ tracers was applied to study the nuclear quadrupole interaction of the first excited $I=1$ state of ^{44}Sc in the cubic bixbyite structure of scandium sesquioxide (Sc_2O_3). In addition, *ab initio* calculations of electronic and structural properties and hyperfine parameters at the cationic sites of the Sc_2O_3 structure were performed using the full-potential augmented plane wave plus local-orbital (APW+lo) method. The accuracy of the calculations and the excellent agreement of the predicted electric-field-gradient (EFG) tensors and the structural properties (lattice parameters, internal positions) with the experimental results enable us to identify the observed hyperfine interactions and to infer the EFG sign that cannot be measured in conventional TDPAC experiments. Additionally, the APW+lo calculations show that the EFG at Sc sites is originated in the population of Sc $3p$ states and give an explanation for the preferential occupation of the asymmetric cationic site C of the structure by the ^{44}Ti doping impurities. Finally, the validity of the ionic model, usually used to describe the EFG at native cation sites, is discussed.

DOI: 10.1103/PhysRevB.82.035206 PACS number(s): 76.80.+y, 71.15.Mb, 71.20.Nr

I. INTRODUCTION

Under suitable conditions, Fe, Mn, Sc, In, Tl, Y, and all the rare-earth elements form a sesquioxide. Polymorphism is common and below about 2300 K, depending on the radius of cation, three polymorphous crystallographic structures have been found:[1] the hexagonal phase (A-type, space group $P\bar{3}m1$), the monoclinic phase (B-type, $C2/m$), and the cubic phase (C-type, $Ia\bar{3}$). At very high temperatures, there are two additional structures. One is hexagonal (H-type, space group $P6_3/mmc$) and the other one is cubic (X-type, $Im\bar{3}m$). The phase stability and phase transitions with temperature or pressure for all the rare-earth sesquioxides were summarized in Ref. 1 and more recently in Ref. 2.

Sesquioxides have broad technological significance.[3–12] For example, they play a vital role in the processing of ceramics as additives for low-temperature sintering, as grain growth inhibitors, and as phase stabilizers, and have potential applications in nuclear engineering and can also be used (due to its luminescent properties) as scintillator materials. More recently, the potential technological applications of magnetic semiconductors to the field of spintronics have motivated the study of many promising systems, including transition-metal-doped semiconducting oxides such as Cr-, Fe- (and other $3d$ transition metals) doped In_2O_3. For all these reasons, electronic and structural properties of rare-earth sesquioxides were extensively studied (see, for example, Refs. 10–21 and references therein).

In the last decade, *ab initio* band-structure calculations have gained an important role in supporting, improving, or confuting experimental results.[22–25] In a reverse way, experimental determinations of theoretical *ab initio* predictions are of fundamental importance for the evaluation of the accuracy of proposed models for structural and electronic properties of solids and to check the validity of approximations performed within the framework of the density-functional theory (DFT). In this sense, the electric-field-gradient tensor (EFG), defined as the second derivative of the electrostatic potential with respect to the spatial coordinates $[d^2V(\mathbf{r})/dx_ix_j]$, is a quantity which is extremely sensitive to the symmetry of the electronic charge density. The EFG can be determined with high accuracy and precision by means of hyperfine techniques. Besides the Mössbauer spectroscopy, the time-differential perturbed-angular-correlation (TDPAC) technique is probably the most common hyperfine interaction method using radioactive nuclei.[26] The EFG is measured through its hyperfine interaction with the nuclear quadrupole moment Q of a suitable probe atom introduced in the material under study. Due to the r^{-3} dependence of the EFG tensor from the charge sources, the EFG is very sensitive to small changes in the electronic charge density close (at subnanoscopic scale) to the probe nucleus, which in turn reflects the probe chemistry with its neighborhood (essentially, with the first neighbors of the probe). For this reason, the EFG tensor can be used as a powerful tool to investigate structural and electronic properties.[25]

Generally, in TDPAC experiments the probe atom is an impurity in the system under study. In these cases, the interpretation of such measurements is not straightforward. In fact, the interpretation of experimental EFG results involves understanding the chemical differences between the probe atom and the ion replaced by the impurity. The experimental results show that the differences between probes and indigenous atoms are manifested in subtle ways that are not well described by simple models, as already pointed out in Refs. 27–29. For an accurate calculation of the EFG at an impurity site, the electronic configuration of the host, perturbed by the presence of the impurity, has to be determined. These calcu-

lations prove not to be trivial and time consuming because different problems (associated to the presence of the impurity in the host system) have to be solved: the simulation of the isolated impurity atom, impurity levels, structural distortions, etc.[25]

Among the sesquioxides, scandium sesquioxide (Sc_2O_3) is a very interesting system to study because one of the Sc isotopes (^{44}Sc) can be used as a TDPAC probe. This is one of the few cases in which the TDPAC probe is not an impurity in the system under study. This isotope is not a usual TDPAC probe and very few experiments were performed using it up to now. In this work, we present an experimental TDPAC and theoretical *ab initio* study of the EFG at both cationic sites of cubic Sc_2O_3. As we will show, the *ab initio* calculations, performed with the augmented plane wave plus local-orbital (APW+lo) method, correctly reproduce the experimental results, enabling us to discuss structural and electronic properties of the Sc_2O_3 semiconducting oxide. The excellent agreement between theory and experiment in this pure system gives a solid basis to extend the theoretical and experimental study to doped bixbyites (experiments performed with other probes in oxides with the bixbyite structure can be found, e.g., in Refs. 20, 21, and 30–32).

This paper is organized as follows: in Sec. II, details on TDPAC spectroscopy, the data analysis, and the sample preparation are briefly discussed. In Sec. III, we describe the structure of the system under study and in Sec. IV the experimental EFG results are reported. In Sec. V, the theoretical approach used is described and the results of the APW +lo calculations are presented and discussed in Sec. VI. Finally, in Sec. VII we present our conclusions.

II. SAMPLE PREPARATION AND TDPAC MEASUREMENTS

The TDPAC technique is based on the determination of the influence of extra-nuclear fields on the correlation between the emission directions of two successive radiations emitted during a nuclear-decay γ-γ cascade. As the TDPAC technique and its applications have been reviewed extensively in the literature (see, for example, Ref. 26), only a very brief description of the method and the experimental setup used in the present experiments will be given here. In order to perform the experiments presented, we made use of the 78-68 keV γ-γ cascade in ^{44}Sc, produced after the electron-capture nuclear decay of the ^{44}Ti isotope. The room-temperature TDPAC experiments were made using a TDPAC camera,[33] which consists of six $LaBr_3$(Ce) scintillators (12 mm diameter and 12 mm height) mounted on XP2020URQ photomultipliers tubes. These scintillators have an excellent energy resolution, and both the 68 and 78 keV lines could just be resolved (see Ref. 34). The time resolution of the spectrometer was 750 ps (full width at half maximum) for these energy windows. The long half life of the intermediate state of about 150 ns makes the detection of delayed coincidences up to about 800 ns feasible. The experimental perturbation functions, $R(t)$, were derived from simultaneously measured coincidence spectra, taken between detectors positioned under 180° and 90°. To analyze the measured perturbation functions, a multiple-site model for nuclear-electric-quadrupole interactions for polycrystalline samples and spin $I=1$ (as is the case of the TDPAC intermediate level of ^{44}Sc) was used,[35]

$$R(t) = A_{22}^{\exp} \sum_i f_i G_{22}^i(t). \tag{1}$$

With

$$G_{22}(t) = \frac{2}{5} + \frac{1}{5}\cos\,\omega_1 t + \frac{1}{5}\cos\,\omega_2 t + \frac{1}{5}\cos\,\omega_3 t, \tag{2}$$

f_i denotes the relative fraction of nuclei that experiences a given perturbation and $A_{22}^{\exp}$ is the effective anisotropy of the γ-γ cascade. The ω_1, ω_2, and ω_3 interaction frequencies are related to the nuclear quadrupole frequency $\omega_Q = eQV_{ZZ}/4\hbar$ by $\omega_1 = 2\eta\omega_Q$, $\omega_2 = (3-\eta)\omega_Q$, $\omega_3 = (3+\eta)\omega_Q$. η is the asymmetry parameter defined as $(V_{XX} - V_{YY})/V_{ZZ}$, where V_{ii} are the principal components of the EFG tensor that are ordered according to $|V_{XX}| < |V_{YY}| < |V_{ZZ}|$. These relations mean that for $\eta=0$, we have only one frequency and an elevated hard core and for $\eta=1$, on the other hand, we have two frequencies: ω_1 and ω_2 coincide and ω_3 is just twice as large as ω_1. In order to account for a finite distribution in ω_Q, which is assumed to be Lorentzian, each of the cosine terms, but not the hard core, is multiplied by a factor $\exp(-\delta\omega_n t)$, where δ denotes the half width at half maximum of the EFG distribution function.

For the present experiments, commercially obtained high-purity Sc_2O_3 powder samples (Aldrich, 99.99% metallic purity) were used. X-ray diffraction analysis of the samples verified that only the crystalline cubic phase was present. In order to introduce the (^{44}Ti→)^{44}Sc probes at free-of-defect cation sites of Sc_2O_3, a carrier-free ^{44}Ti in 4 M HCl solution was dropped onto the Sc_2O_3 powder and then dried with an infrared lamp. After that, the samples underwent a diffusion thermal treatment at 973 K for 2 h. The TDPAC results showed that after this treatment, at least 95% of the probes resided on regular Sc sites. The activity of the final sample was about 5 μCi. Due to this low activity and the large half-life of ^{44}Ti (60 years), the spectra were accumulated during 1 month.

III. BIXBYITE STRUCTURE

Scandium sesquioxide crystallizes in the cubic bixbyite phase. This form takes its name from the mineral $(Fe,Mn)_2O_3$, called bixbyite. In this structure, the cations form a nearly cubic face-centered lattice (space group $Ia\bar{3}$) in which six out of the eight tetrahedral sites are occupied by oxygen atoms. The unit cell of the oxide lattice consists of eight such cubes, containing 32 cations and 48 O^{-2} ions. Two nonequivalent sites for the cations, called C and D, both O_6 coordinated, characterize the structure. Their relative abundance in the lattice is $f^C/f^D = 3$. The site D is axially symmetric and can be locally described as a cation surrounded by six oxygen atoms at the corners of a distorted cube, leaving two corners of one diagonal free ($D3d$ point-group symmetry). In the C site, the cube is more distorted ($C2$ symmetry)

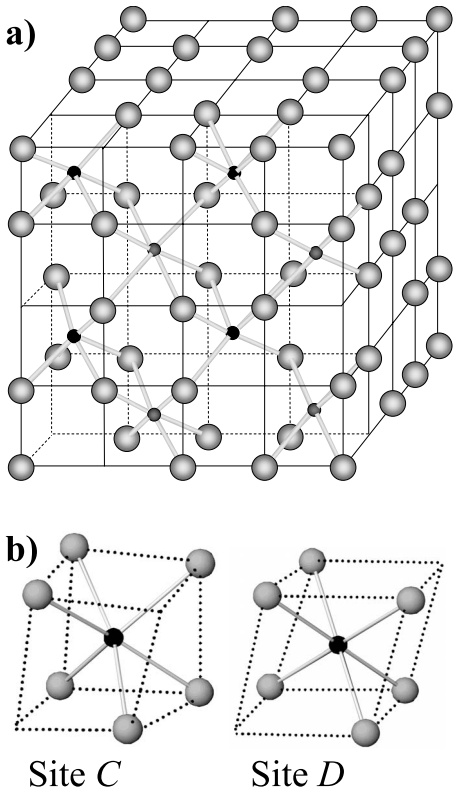

FIG. 1. (a) Idealized crystal structure of Sc_2O_3. Note two types of octahedral cation sites in alternating layers. (b) Nearest-neighbor oxygen (gray spheres) distribution around each cationic site (black spheres) in the bixbyite structure.

and the six oxygen atoms leave free two corners on a face diagonal.[1,36] In Fig. 1, we show the idealized crystal structure of Sc_2O_3 and the distribution of the oxygen ions around each nonequivalent cationic site. Concerning the anions, there is only one crystallographic site, coordinated to four cations. The positions of all the atoms in the unit cell are determined by four internal parameters u,x,y,z, which determine the positions of the Sc atoms at the C site:

$$\pm(u\ 0\ 1/4;1/4\ u\ 0;0\ 1/4\ u;-u\ 1/2\ 1/4;1/4\ -u\ 1/2;1/2\ 1/4-u),$$

B.C. and those of the oxygen atoms:

$$\pm(x\ y\ z;x\ -y\ 1/2-z;1/2-x\ y-z;-x\ 1/2\ -y\ z;z\ x\ y;1/2-z\ x-y;-z\ 1/2-x\ y;z\ -x\ 1/2\ -y;y\ z\ x;-y\ 1/2-z\ x;y-z\ 1/2-x;1/2-y\ z\ -x),$$

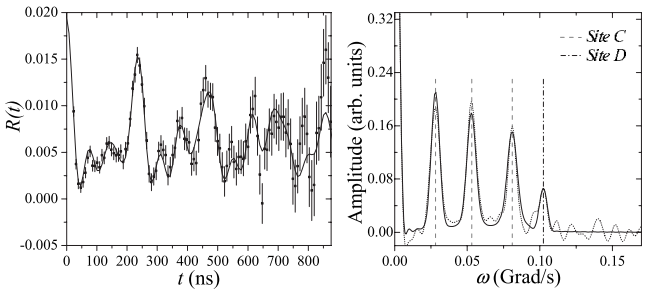

FIG. 2. $R(t)$ spectrum (left) and their corresponding cosine transform (right) of (^{44}Ti→)^{44}Sc in cubic Sc_2O_3 measured at 300 K. The frequencies ω_n associated with the hyperfine interactions HFIC and HFID are indicated in the Fourier spectrum.

B.C. The D-type Sc atoms are located at $\pm(1/4\ 1/4\ 1/4;1/4\ 3/4\ 3/4;3/4\ 1/4\ 3/4;3/4\ 3/4\ 1/4)$, B.C. The notation "B.C." indicates that the group of coordinates has to be repeated adding (1/2 1/2 1/2). The experimentally determined internal and lattice parameters are $u=-0.03546$, $x=0.39137$, $y=0.15477$, $z=0.38137$, and $a=9.845$ Å, respectively.[37]

According to the geometry of this structure, we expect two clearly distinguishable hyperfine interactions for probes located at each cation sites. That corresponding to site C will be characterized by $\eta_C>0.5$ while $\eta_D=0.0$ and $\omega_Q^d \cong 2\omega_Q^C$ will characterize the symmetric site D. According to the relative abundance of each site in the lattice, the first one should be present with triple intensity.

IV. EXPERIMENTAL RESULTS

Figures 2(a) and 2(b) show the $R(t)$ spectrum and their corresponding Fourier transform, taken at 300 K in air. The solid line in the $R(t)$ spectrum is the best least-squares fit of Eq. (1) to the experimental data. The solid line in the frequency spectrum comes from the cosine transform of the $R(t)$ fit. Two hyperfine interactions, labeled HFIC and HFID, were necessary in order to reproduce the experimental $R(t)$ spectrum. The parameter values that characterize both interactions are listed in Table I. As can be seen, both hyperfine interactions are very well defined ($\delta<3.0\%$). The asymmetry parameter of HFID is equal to zero whereas a high η value for HFIC (see Table I) was found, as expected from the coordination symmetries of sites D and C, respectively. In addition, the frequency of the axially symmetric interaction is twice as large as that of the asymmetric one. Furthermore, the fraction of the C site which corresponds to the sum of the

TABLE I. Results of least-squares fits of Eq. (1) to the $R(t)$ spectrum displayed in Fig. 2. When no errors are quoted it means that the parameter was kept fixed during the fitting procedure. In order to calculate V_{ZZ} from the experimental nuclear quadrupole frequency ω_Q, the quadrupole moment $Q(^{44}\mathrm{Sc}, I=1) = \pm 0.214(3)$ b(Ref. 34) was used. The sign of the experimental ω_Q (and hence V_{ZZ}) are unknown.

	f (%)	ω_Q (Mrad/s)	η	δ (%)	V_{ZZ} (10^{21} V/m^2)
HFID	11(2)	34.1(2)	0.00	0	4.19(2)
HFIC	89(2)	22.31(6)	0.630(3)	2.6(4)	2.741(7)

three lowest peak areas is much larger than that of the *D* site. It is then clear that HFIC and HFID can be undoubtedly assigned to probes located at the defect-free cationic sites *C* and *D* of the crystalline bixbyite structure.

The relative population of the two sites should be $f^C/f^D=3$ if the cationic sites were occupied according to their natural abundance in the crystalline structure. In the present experiments, the experimental ratio f^C/f^D was larger than this value, indicating a preferential occupation of site *C*. A departure of the $f^C/f^D=3$ was already observed in the case of the TDPAC probe $^{181}\mathrm{Hf}\rightarrow{}^{181}\mathrm{Ta}$ in Sc_2O_3 and other bixbyites (in these cases, $f^C/f^D<3$ was found). This behavior was explained in the past in terms of the relative ionic size of the probe and the cationic "space" in the host.[20,38] We will discuss the preferential occupation of site *C* in Sec. VI E.

V. *AB INITIO* CALCULATIONS: PROCEDURE

Theoretical calculations based on the DFT (Ref. 39) were performed with the WIEN2K implementation[40] of the APW +lo (Refs. 41–43) method in a scalar relativistic version. Exchange and correlation effects were treated within density-functional theory using both the local-density (LDA, Ref. 44), the generalized-gradient approximation (GGA, Ref. 45), and the GGA recently proposed by Wu and Cohen (WC-GGA, Ref. 46), which yields, on average, better results for solids than the standard GGA.[47] In this method, the wave functions are expanded in spherical harmonics inside non-overlapping atomic spheres of radius R_{MT} and in plane waves in the remaining space of the unit cell (the interstitial region). The atomic sphere radii used for Sc and O were 1.06 Å and 0.96 Å, respectively. The parameter RK_{max}, which controls the size of the basis set, was set to 8. Integration in reciprocal space was performed using the tetrahedron method taking up to 200 *k* points in the full Brillouin zone (BZ), which are reduced to 11 *k* points in the irreducible wedge of the BZ (IWBZ). To plot the density of states (DOS), we calculated eigenvalues at a denser mesh of 500 *k* points (24 *k* points in the IWBZ). To improve linearization, we also introduced local orbitals to include Sc 4*s* and Sc 3*p* and O 2*s* orbitals.[48] In order to obtain the equilibrium positional parameters *u*, *x*, *y*, and *z*, once self-consistency of the potential was achieved, quantum-mechanically-derived forces on the ions were obtained, they were displaced according to a Newton-damped scheme, and the new positions for the atoms were obtained (for details see Ref. 25 and references therein). This procedure was repeated until the forces on the ions were below a tolerance value of 0.005 eV/Å. The correctness of the choice of all these parameters was checked by performing calculations for other R_{MT}'s, *k*-point sampling, and RK_{max} values. In our calculations, the $V_{i,j}$ elements of the EFG tensor were obtained directly from the V_{2M} components of the lattice harmonic expansion of the Coulomb potential.[49] The convergence errors in the V_{ii} components are in the order of 10^{20} V/m^2.

VI. THEORETICAL RESULTS

A. Electronic structure

Initially, the lattice parameter and the atomic positions were fixed at their experimental values. The calculated band structure and the DOS of Sc_2O_3 are shown in Figs. 3 and 4, respectively. The DOS and the overall band structure obtained here are consistent with previous theoretical results obtained in In_2O_3 and other isomorphous rare-earth sesquioxides.[10,13,14,50,51] All the functionals used in the APW calculations predict a similar direct (minimum) band gap of about 4.0 eV at the Γ point (see Fig. 3). This calculated band gap is about 1.7 eV smaller than the measured gap, 5.7 eV.[52] This underestimation of the band gap, especially in metal oxides, reflects the well-known deficiency of LDA and GGA

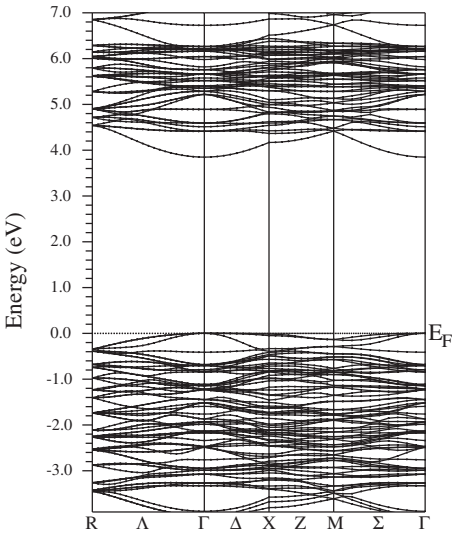

FIG. 3. Calculated band structure for the system Sc_2O_3. Zero energy is at the Fermi level (E_F), denoted by a solid horizontal line.

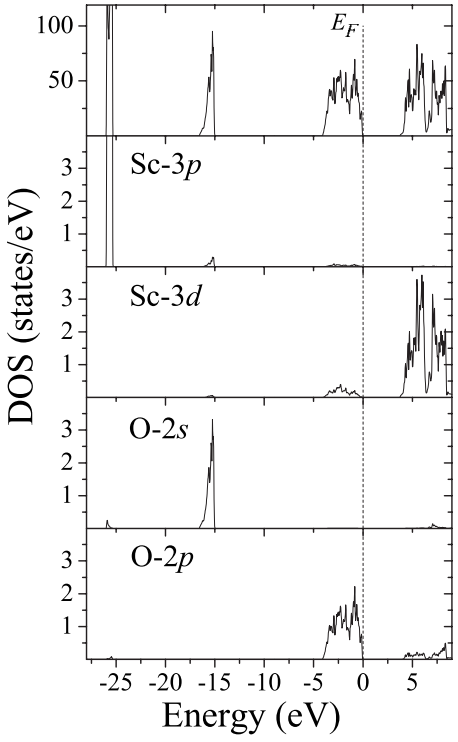

FIG. 4. Calculated total and partial densities of states of Sc_2O_3. Energies are referred to the Fermi level (E_F), denoted by a vertical dashed line.

TABLE II. Lattice parameter a and atomic internal coordinates u, x, y, and z of the bixbyite structure of Sc_2O_3 obtained in our APW+lo calculations compared to the experimental values (Ref. 37).

	a (Å)	u	x	y	z
LDA	9.708	−0.0364	0.3915	0.1545	0.3810
GGA	9.900	−0.0362	0.3914	0.1545	0.3812
WC-GGA	9.798	−0.0361	0.3913	0.1543	0.3812
Experimental	9.845	−0.03546	0.39137	0.15477	0.38137

to predict experimental band gaps[53] but this does not invalidate the fine structure of the bands and the calculation of observables, which depend only on the ground state as, for example, the EFG and the atomic coordinates.

Figure 4 shows the DOS and the local DOS projected onto the C-type Sc and O atoms (the projected DOS for the D-type Sc atom is quite analogous). The total DOS is composed of three valence bands: The narrow band located at about −26 eV is the Sc $3p$ band. There is a very small contribution of O $2s$ at these energies but the O $2s$ states form a narrow band located at −15 eV. The upper band, located between −4.5 eV and the Fermi level (adjusted to zero energy) is dominated by O $2p$ states. However, there is a smaller contribution of Sc $3d$ orbitals. This small mixture evidences the ionic nature of the Sc-O bond in agreement with the picture of scandium sesquioxide as an ionic insulator with some degree of covalent bonding between Sc and O atoms.[54] Above the Fermi level, the conduction band is predominantly Sc $3d$ with an admixture of O $2p$ states.

B. Structural properties

After these calculations, the equilibrium lattice parameter and the positional parameters u, x, y, and z of Sc_2O_3 were calculated. As a first step of this structural refinement, the lattice parameter was determined. To do this, the parameters u, x, y, and z were kept fixed to their experimental values and we calculated the energy of the system as a function of the equilibrium volume. Then we fixed the lattice parameter to that corresponding to the minimum energy and the atomic positions were relaxed by force minimization. This cycle must be repeated, i.e., to keep fixed the new internal positions and determine the second equilibrium volume. This new determination of the equilibrium volume gives a value of the lattice parameter that is identical to that corresponding to the first refinement (the difference between both lattice parameters is within the convergence error) so the minimization of the lattice parameter and the internal coordinates can be stopped at this stage. As can be seen in Table II, the lattice parameter and the u, x, y, and z parameters are in excellent agreement with the experimental data. Additionally, the results obtained using LDA, GGA, and WC-GGA approximations are very similar.

C. Electric-field gradients

In this section, we will concentrate on the calculated EFGs at the Sc sites. As far as we know, no experimental values for the EFG at oxygen sites in Sc_2O_3 have been reported. For a complete description of this system, we also included in Table III the results for the EFG at the oxygen site. The EFGs were derived for two different sets of positions: the experimental coordinates and lattice parameter and at those positions predicted by our refinements. The results obtained using the experimental positions are reported in Table III (upper). It is important to note that LDA, GGA, and WC-GGA calculations predict the same EFG when the experimental lattice and internal parameters are used. Due to the fact that the EFG is very sensitive to small changes in the electronic charge density, it is concluded that the description of the electronic structure predicted by these three functionals is almost identical. As can be seen in Table III, the agreement between our APW+lo predictions for the EFG at the Sc sites with the experimental results is excellent.

As mentioned above, the EFG is very sensitive to very small changes in the atomic positions. Even for pure materials, for which accurate structural parameters are available, the spread of the experimental positions could be large enough to change the calculated EFG values. For this reason, we performed calculations using the theoretically predicted equilibrium lattice parameters and positional parameters u, x, y, and z. As can be seen in Table III (middle part), the mayor component of the EFG tensor (V_{ZZ}) does not vary so much when the experimentally determined structural parameters are exchanged by the theoretical ones. Only a small reduction in the asymmetry parameter at site C is observed. The agreement between theory and experiment is excellent, showing the capability of the APW+lo method to correctly described electronic and structural properties in Sc_2O_3.

In order to understand the origin of the EFG tensor, we have to take into account that the EFG tensor is directly related to the anisotropy of the electronic density in the vicinity of the nucleus of the probe atom where the EFG tensor is calculated or measured. In the APW+lo model, the EFG can be decomposed into two terms:[55] the first one is named the valence contribution since it originates from the nonspherical electron density of the valence and semicore electrons within the muffin-tin sphere of the probe atom. The second contribution is the lattice contribution originating from more distant regions of the crystal. In the case of Sc_2O_3, as in almost all the cases, the valence contribution to the EFG dominates while the lattice term is almost negligible (this last contribution accounts for less than 5% of the total EFG). For this reason, to investigate the origin of the EFG, we concentrate on the valence contribution to the EFG. This dominant contribution can be further decomposed according to the different orbital symmetries. Table IV contains the total valence contribution to V_{ii} and its components arising

TABLE III. V_{ZZ} and asymmetry parameter η at the Sc and O sites obtained in the APW+lo calculations compared with experimental TDPAC results at 300 K.

	From experimental structural parameters (Refs. 37 and 38)					
	Site *D*		Site *C*		Oxygen site	
	V_{ZZ} $[10^{21}$ V/m$^2]$	η	V_{ZZ} $[10^{21}$ V/m$^2]$	η	V_{ZZ} $[10^{21}$ V/m$^2]$	η
LDA	+4.53	0.00	−2.99	0.71	+1.45	0.49
GGA	+4.57	0.00	−2.98	0.68	+1.40	0.56
WC-GGA	+4.58	0.00	−2.96	0.69	+1.42	0.52
	From structural parameters refined by APW+lo (this work)					
	Site *D*		Site *C*		Oxygen site	
	V_{ZZ} $[10^{21}$ V/m$^2]$	η	V_{ZZ} $[10^{21}$ V/m$^2]$	η	V_{ZZ} $[10^{21}$ V/m$^2]$	η
LDA	+4.80	0.00	−3.02	0.52	+1.44	0.46
GGA	+4.48	0.00	−2.95	0.54	+1.32	0.57
WC-GGA	+4.57	0.00	−2.91	0.54	+1.36	0.60
	Experimental results					
	Site *D*		Site *C*			
	V_{ZZ} $[10^{21}$ V/m$^2]$	η	V_{ZZ} $[10^{21}$ V/m$^2]$	η		
	4.19(2)	0.00	2.741(7)	0.630(3)		

from *p*, *d*, and *s-d* orbital symmetries (higher *l* contributions are negligible). As can be seen, the *p* contribution dominates over the *d* contribution. The charge density originating from *p* wave functions dominates over the *d* contributions because the first node of the *p* wave function is at much shorter distance than the one of the *d* wave function (see Ref. 55). This behavior has also been seen in other binary oxides doped with Cd and Ta.[25,28,29]

D. Comparison with other calculations

It is well known (and our results confirm this fact) that the bonding in these sesquioxides is mainly ionic.[54] In the case of mainly ionic compounds, the simplest and most widely used approximation for the calculation of the EFG at a probe atom is the point-charge model (PCM).[16] In this approximation, the EFG tensor at the probe site is given by $V_{ii}^{\mathrm{PCM}}=(1-\gamma_\infty)V_{ii}^{latt}$, where V_{ii}^{latt} is the EFG tensor originating from the nominal-valence point charges located at the ion positions in the lattice and γ_∞ is the Sternheimer antishielding factor,[16] which depends only on the probe. Using the lattice parameter and the atomic coordinates coming from the x-ray determinations and using a value of $\gamma_\infty=-11.48$ (Ref. 56), the PCM gives $V_{ZZ}=+2.9\times10^{21}$ V/m^2, $\eta=0.00$ for site *D* and $V_{ZZ}=-1.6\times10^{21}$ V/m^2, $\eta=0.95$ for site *C*. Compared with the results reported in Table III, the agreement between the PCM

TABLE IV. *p*, *d*, and *s-d* valence contributions to the EFG at both Sc sites in Sc_2O_3, in units of 10^{21} V/m^2. The results correspond to LDA calculations using the lattice parameters and *u*, *x*, *y*, and *z* parameters predicted by the APW+lo calculations (very similar results were obtained using the GGA and the WC-GGA approximations for the exchange and correlation potential).

	Site *D*			Site *C*		
	V_{ZZ}	V_{YY}	V_{XX}	V_{ZZ}	V_{YY}	V_{XX}
p	+4.16	−2.08	−2.08	−2.77	+2.38	+0.39
d	+0.40	−0.20	−0.20	−0.16	+0.12	+0.04
s-d	−0.02	+0.01	+0.01	+0.01	0.00	−0.01
Total valence	+4.54	−2.27	−2.27	−2.92	+2.50	+0.42

and the APW+lo predictions (and of course with the experimental results) is poor. Even if the APW+lo predictions for the equilibrium lattice parameter and u, x, y, and z parameters are introduced in the PCM calculations this model still fails in the prediction of the EFG tensor at Sc sites. In order to understand the failure of the PCM in this pure and highly ionic oxide, we will compare the PCM and APW+lo models. At this point, it is important to mention that valence and lattice contributions to the EFG in the *ab initio* approach are not identical to the generally named "valence" and "lattice" contributions in point-charge-based models. But it is possible to make a connection between these two scenarios. In the case of the PCM model, the EFG can be written as

$$V_{ZZ}^{\mathrm{PCM}} = -\gamma_{\infty} V_{ZZ}^{latt,\mathrm{PCM}} + V_{ZZ}^{latt,\mathrm{PCM}}. \tag{3}$$

On the other hand, in the APW+lo framework we have

$$V_{ZZ}^{\mathrm{APW+lo}} = V_{ZZ}^{val} + V_{ZZ}^{latt,\mathrm{APW+lo}} = V_{ZZ}^{val,p} + V_{ZZ}^{val,d} + V_{ZZ}^{latt,\mathrm{APW+lo}}. \tag{4}$$

In both models, the bare lattice contribution is negligible. Taking into account the orbital involved in the γ_{∞} factor (essentially, Sc $3d$ orbitals), we can correlate the term $\gamma_{\infty} V_{ZZ}^{latt,\mathrm{PCM}}$ with the d valence contribution in the APW+lo model. In this way, the PCM overestimate the d contribution to the EFG and the p contribution (the dominating one according to APW+lo) is neglected. In conclusion, the discrepancy between the PCM and the APW+lo results can be attributed to an erroneous description of the electronic structure of the system, in particular, in the subnanoscopic neighborhood of the impurity.

E. Site occupation

As mentioned before, if both cationic sites are randomly occupied by the ^{44}Ti($\rightarrow{}^{44}$Sc) probes, the ratio f^C/f^D must be equal to 3. However, in the experiment we found $f^C/f^D \cong 5$. In other words, we found a preferential occupation of the C site by the TDPAC probes ^{44}Ti. In order to explain this departure from the natural cationic site population, we have to concentrate on the radioactive father of ^{44}Sc, the ^{44}Ti isotope, which determines the site occupation.

To understand the preference of the probe ^{44}Ti($\rightarrow{}^{44}$Sc) for site C, we performed *ab initio* calculations in Ti-doped Sc_2O_3, assuming that Ti substitutionally replaces a Sc ion at site D or at site C. Calculations were performed with the same precision than those corresponding to pure Sc_2O_3. We have to mention that the total energy requires a larger number of plane waves and of k points for convergence. However, the energy differences are well converged for the employed parameters. The structural distortions induced by the Ti impurities in the Sc_2O_3 host were computed and different charge states of the impurities (see Ref. 25) were considered. We found that (independent of the charge state of the impurity and the parameterization employed for the exchange and correlation potential), when a Ti impurity replaces a C-type Sc, the energy of the system $Sc_{31}TiO_{48}$ is 1.5 eV lower than those corresponding to the system $Sc_{31}TiO_{48}$ with a Ti located at a D site. This result explains the preference of the probe ^{44}Ti($\rightarrow{}^{44}$Sc) for site C. This preference for the C site was found for other dopants in oxides with the bixbyite structure as well.[57]

VII. SUMMARY AND CONCLUSIONS

Density-functional calculations of the electronic structure and atomic forces have been used to study the semiconductor Sc_2O_3 (cubic bixbyite structure) in its pure form. Energy minimization and force calculations were used to refine the structure, and from the self-consistent potential the electric-field gradients were obtained. These calculations allowed a comparison of theoretical predictions to experimental results obtained by x-ray diffraction reported in the literature and by TDPAC measurements performed with the unconventional probe $^{44}\mathrm{Ti} \rightarrow {}^{44}\mathrm{Sc}$. We found that LDA, GGA, and WC-GGA correctly predict the semiconducting nature of Sc_2O_3. Due to the well-known DFT error in predicting fundamental energy gaps, all approximations lead to band-gap values 1.7 eV smaller than the experimental one and otherwise make a similar description of the electronic structure of Sc_2O_3 semiconductor.

Our results for the structural properties are in excellent agreement with the experimental ones. Concerning the hyperfine parameters, the combination of the TDPAC experiments and the calculations enables the complete EFG characterization at both nonequivalent cationic sites of the Sc_2O_3 structure. The magnitude and symmetry of the EFG are in excellent agreement with the TDPAC results. These agreements enable us to infer the sign of the EFGs (negative EFG for the asymmetric site and positive for the symmetric one) with high reliability. We also found that the EFG tensor is mainly originated in the population of Sc orbitals with p symmetry. Finally, we showed that a simple model for the EFG, such as the PCM, using experimental or the APW+lo predictions for the structural parameters, does not reproduce the EFG magnitude and symmetry. The discrepancy between the PCM and the experimental and APW+lo results is originated in the bad description of the dominant valence contribution to the EFG. From our results it is clear that the problem of the EFG at cationic sites, even in pure and highly ionic oxides, is too complicated to be described by simple models such as the PCM with antishielding factors.

APW+lo calculations performed in Ti-doped Sc_2O_3, assuming that Ti substitutionally replaces both types of Sc atoms, show that the radioactive father of ^{44}Sc, the ^{44}Ti isotope, prefers to locate at the C-type cations, a result that explains the preferential occupation of the C site observed in our TDPAC experiments.

In a behavior similar to what has been observed with other binary oxides, our results suggest that a suitable combination of very accurate theoretical and experimental EFG determinations can be used as a powerful tool to probe electronic and structural properties with a very high degree of accuracy. Additionally, the excellent agreement between theory and experiment gives a solid base for the study of Cd- or Ta-doped Sc_2O_3, necessary to explain the TDPAC results found using these widely used probes. These calculations are now in progress.

ACKNOWLEDGMENTS

This work was partially supported by Agencia Nacional de Promoción Científica y Tecnológica (ANPCyT) under Grant No. PICT98 03-03727, Consejo Nacional de Investigaciones Científicas y Técnicas (CONICET, PIPs 0002 and 6032), Fundación Antorchas, Argentina, and the Third World Academy of Sciences (TWAS, Italy, RGA 97-057). This research made use of the HP-Parallel-Computing Bose Cluster, and the computational facilities of the Physics of Impurities (PhI) group at IFLP and Departamento de Física (UNLP).

[1] L. Eyring, in *Handbook on the Physics and Chemistry of Rare Earths*, edited by K. A. Gschneidner and L. Eyring (North-Holland, Amsterdam, 1979), p. 337.
[2] M. Zinkevich, Prog. Mater. Sci. **52**, 597 (2007).
[3] J. B. Gruber, M. E. Hills, M. D. Seltzer, S. B. Stevens, and C. A. Morrison, J. Appl. Phys. **72**, 5253 (1992).
[4] J. Li, T. Ikegami, and T. Mori, J. Am. Ceram. Soc. **88**, 817 (2005).
[5] M. Tang, P. Lu, J. A. Valdez, and K. E. Sickafus, J. Appl. Phys. **99**, 063514 (2006).
[6] B. Antic, M. Mitric, and D. Rodic, J. Magn. Magn. Mater. **145**, 349 (1995).
[7] V. Skrikanth, A. Sato, J. Yoshimoto, J. H. Kim, and T. Ikegami, Cryst. Res. Technol. **29**, 981 (1994).
[8] A. Lempicki, C. Brecher, P. Szupryczynski, H. Lingertat, V. Nagarkar, S. Tipnis, and S. Miller, Nucl. Instrum. Methods Phys. Res. A **488**, 579 (2002).
[9] J. Philip, A. Punnoose, B. I. Kim, K. M. Reddy, S. Layne, J. O. Holmes, B. Satpati, P. R. Leclair, T. S. Samtos, and J. S. Moodera, Nature Mater. **5**, 298 (2006).
[10] P. D. C. King, T. D. Veal, F. Fuchs, Ch. Y. Wang, D. J. Payne, A. Bourlange, H. Zhang, G. R. Bell, V. Cimalla, O. Ambacher, R. G. Egdell, F. Bechstedt, and C. F. McConville, Phys. Rev. B **79**, 205211 (2009), and references therein.
[11] F. Matino, L. Persano, V. Arima, D. Pisignano, R. I. R. Blyth, R. Cingolani, and R. Rinaldi, Phys. Rev. B **72**, 085437 (2005), and references therein.
[12] R. P. Panguluri, P. Kharel, C. Sudakar, R. Naik, R. Suryanarayanan, V. M. Naik, A. G. Petukhov, B. Nadgorny, and G. Lawes, Phys. Rev. B **79**, 165208 (2009); L. X. Guan, J. G. Tao, Z. R. Xiao, B. C. Zhao, X. F. Fan, C. H. A. Huan, J. L. Kuo, and L. Wang, *ibid.* **79**, 184412 (2009).
[13] A. Walsh, J. L. F. Da Silva, S. H. Wei, C. Körber, A. Klein, L. F. J. Piper, Alex DeMasi, Kevin E. Smith, G. Panaccione, P. Torelli, D. J. Payne, A. Bourlange, and R. G. Egdell, Phys. Rev. Lett. **100**, 167402 (2008).
[14] L. Petit, A. Svane, Z. Szotek, and W. M. Temmerman, Phys. Rev. B **72**, 205118 (2005).
[15] J. Shitu, D. Wiarda, T. Wenzel, M. Uhrmacher, K. P. Lieb, S. Bedi, and A. Bartos, Phys. Rev. B **46**, 7987 (1992).
[16] D. Wiarda, M. Uhrmacher, A. Bartos, and K. P. Lieb, J. Phys.: Condens. Matter **5**, 4111 (1993).
[17] A. Bartos, D. Wiarda, M. Uhrmacher, and K. P. Lieb, Hyperfine Interact. **80**, 953 (1993).
[18] L. A. Errico, M. Rentería, G. Fabricius, and G. N. Darriba, Hyperfine Interact. **158**, 63 (2004).
[19] L. A. Errico, M. Rentería, A. G. Bibiloni, and G. N. Darriba, Phys. Status Solidi C **2**, 3576 (2005).
[20] L. A. Errico, M. Rentería, A. F. Pasquevich, A. G. Bibiloni, and K. Freitag, Eur. Phys. J. B **22**, 149 (2001).
[21] L. A. Errico, M. Rentería, A. G. Bibiloni, and K. Freitag, Physica B **389**, 124 (2007).
[22] S. Lany, P. Blaha, J. Hamann, V. Ostheimer, H. Wolf, and T. Wichert, Phys. Rev. B **62**, R2259 (2000).
[23] P. Blaha, K. Schwarz, W. Faber, and J. Luitz, Hyperfine Interact. **126**, 389 (2000).
[24] L. A. Terrazos, H. M. Petrilli, M. Marszalek, H. Saitovich, P. R. J. Silva, P. Blaha, and K. Schwarz, Solid State Commun. **121**, 525 (2002).
[25] L. A. Errico, G. Fabricius, M. Rentería, P. de la Presa, and M. Forker, Phys. Rev. Lett. **89**, 055503 (2002); L. A. Errico, G. Fabricius, and M. Rentería, Phys. Rev. B **67**, 144104 (2003).
[26] G. Schatz and A. Weidinger, *Nuclear Condensed Matter Physics: Nuclear Methods and Applications* (Wiley, Chichester, England, 1996); E. N. Kaufmann and R. J. Vianden, Rev. Mod. Phys. **51**, 161 (1979); A. Lerf and T. Butz, Angew. Chem., Int. Ed. Engl. **26**, 110 (1987).
[27] J. M. Adams and G. L. Catchen, Phys. Rev. B **50**, 1264 (1994).
[28] R. E. Alonso, L. A. Errico, E. L. Peltzer y Blancá, A. López-García, A. Svane, and N. E. Christensen, Phys. Rev. B **78**, 165206 (2008).
[29] G. N. Darriba, L. A. Errico, P. D. Eversheim, G. Fabricius, and M. Rentería, Phys. Rev. B **79**, 115213 (2009).
[30] A. W. Carbonari, J. Mestnik-Filho, R. N. Attili, M. Moralles, and R. N. Saxena, Hyperfine Interact. **120-121**, 475 (1999).
[31] D. Khabibulin, K. Romanenko, M. Zuev, and O. Lapina, Magn. Reson. Chem. **45**, 962 (2007).
[32] E. L. Muñoz, D. Richard, L. A. Errico, and M. Rentería, Physica B **404**, 2757 (2009).
[33] T. Butz, S. Saibene, Th. Fraenzke, and M. Weber, Nucl. Instrum. Methods Phys. Res. A **284**, 417 (1989).
[34] S. B. Ryu, S. K. Das, T. Butz, W. Schmitz, Ch. Spiel, P. Blaha, and K. H. Schwarz, Phys. Rev. B **77**, 094124 (2008).
[35] T. Butz, Hyperfine Interact. **52**, 189 (1989); **73** (E), 387 (1992).
[36] M. Marezio, Acta Crystallogr. **20**, 723 (1966).
[37] R. W. G. Wyckoff, *Crystal Structures* (Wiley Interscience, New York, 1964), Vol. 2 for the lattice parameter; R. Norrestam, Ark. Kemi **29**, 343 (1968) for the internal parameters.
[38] M. Rentería, A. G. Bibiloni, F. G. Requejo, A. F. Pasquevich, J. Shitu, L. A. Errico, and K. Freitag, Mod. Phys. Lett. B **12**, 819 (1998).
[39] S. Cottenier, *Density Functional Theory and the Family of (L)APW Methods: A Step-by-Step Introduction* (Instituut voor Kern- en Stralingsfysica, KU Leuven, Belgium, 2002).
[40] P. Blaha, K. Schwarz, G. Madsen, D. Kvasnicka, and J. Luitz, *WIEN2k, An Augmented Plane Wave Plus Local Orbitals Program for Calculating Crystal Properties*, edited by K. Schwarz (Technical Universität Wien, Austria, 1999).

[41] E. Sjöstedt, L. Nordström, and D. J. Singh, Solid State Commun. **114**, 15 (2000).
[42] G. K. H. Madsen, P. Blaha, K. Schwarz, E. Sjöstedt, and L. Nordström, Phys. Rev. B **64**, 195134 (2001).
[43] P. Hohenberg and W. Kohn, Phys. Rev. **136**, B864 (1964); W. Kohn and L. J. Sham, *ibid.* **140**, A1133 (1965).
[44] J. P. Perdew and Y. Wang, Phys. Rev. B **45**, 13244 (1992).
[45] J. P. Perdew, K. Burke, and M. Ernzerhof, Phys. Rev. Lett. **77**, 3865 (1996).
[46] Z. Wu and R. E. Cohen, Phys. Rev. B **73**, 235116 (2006).
[47] F. Tran, R. Laskowski, P. Blaha, and K. Schwarz, Phys. Rev. B **75**, 115131 (2007).
[48] P. Blaha, D. J. Singh, P. I. Sorantin, and K. Schwarz, Phys. Rev. B **46**, 1321 (1992).
[49] K. Schwarz, C. Ambrosch-Draxl, and P. Blaha, Phys. Rev. B **42**, 2051 (1990).
[50] F. X. Zhang, M. Lang, J. W. Wang, U. Becker, and R. C. Ewing, Phys. Rev. B **78**, 064114 (2008).
[51] L. Marsella and V. Fiorentini, Phys. Rev. B **69**, 172103 (2004).
[52] C. T. Horovitz and G. A. Gschneidner, *Scandium* (Academic Press, New York, 1975), p. 115; H. J. Borchardt, J. Chem. Phys. **39**, 504 (1963).
[53] See, e.g., W. G. Aulbur, L. Jönsson, and J. W. Wilkins, Solid State Phys. **54**, 1 (1999).
[54] B. M. Angelov, J. Phys. C **10**, L505 (1977); **15**, L239 (1982).
[55] P. Blaha, K. Schwarz, and P. H. Dederichs, Phys. Rev. B **37**, 2792 (1988).
[56] F. D. Feiock and W. R. Johnson, Phys. Rev. **187**, 39 (1969).
[57] C. R. Stanek, K. J. McClellan, B. P. Uberuaga, K. E. Sickafus, M. R. Levy, and R. W. Grimes, Phys. Rev. B **75**, 134101 (2007).